

Cutaneous Retinoic Acid Levels Determine Hair Follicle Development and Downgrowth^{*S}

Received for publication, July 5, 2012, and in revised form, September 12, 2012. Published, JBC Papers in Press, September 24, 2012, DOI 10.1074/jbc.M112.397273

Junko Okano[‡], Clara Levy[‡], Ulrike Licht[§], Hong-Wei Sun[¶], Stuart H. Yuspa[§], Yasuo Sakai^{||}, and Maria I. Morasso^{‡1}

From the [‡]Developmental Skin Biology Section, NIAMS, the [§]Laboratory of Cancer Biology and Genetics, NCI, and the [¶]Biodata Mining and Discovery Section, NIAMS, National Institutes of Health, Bethesda, Maryland 20892 and the ^{||}Department of Plastic Surgery, Osaka University School of Medicine, Suita, Osaka, 565-0871, Japan

Background: Excess retinoic acid (RA) leads to hair loss, but the effect of RA during embryonic hair follicle development is unknown.

Results: Mice lacking the RA-degrading enzyme *Cyp26b1* in skin exhibit major hair follicle development defects.

Conclusion: RA levels determine downgrowth and bending of the hair follicle.

Significance: These data identify crucial developmental signaling pathways and transcriptional regulators as targets regulated by RA during hair follicle morphogenesis.

Retinoic acid (RA) is essential during embryogenesis and for tissue homeostasis, whereas excess RA is well known as a teratogen. In humans, excess RA is associated with hair loss. In the present study, we demonstrate that specific levels of RA, regulated by *Cyp26b1*, one of the RA-degrading enzymes, are required for hair follicle (hf) morphogenesis. Mice with embryonic ablation of *Cyp26b1* (*Cyp26b1*^{−/−}) have excessive endogenous RA, resulting in arrest of hf growth at the hair germ stage. The altered hf development is rescued by grafting the mutant skin on immunodeficient mice. Our results show that normalization of RA levels is associated with reinitiation of hf development. Conditional deficiency of *Cyp26b1* in the dermis (*En1Cre; Cyp26b1f*−) results in decreased hair follicle density and specific effect on hair type, indicating that RA levels also influence regulators of hair bending. Our results support the model of RA-dependent dermal signals regulating hf downgrowth and bending. To elucidate target gene pathways of RA, we performed microarray and RNA-Seq profiling of genes differentially expressed in *Cyp26b1*^{−/−} skin and *En1Cre;Cyp26b1f*− tissues. We show specific effects on the Wnt-catenin pathway and on members of the Runx, Fox, and Sox transcription factor families, indicating that RA modulates pathways and factors implicated in hf downgrowth and bending. Our results establish that proper RA distribution is essential for morphogenesis, development, and differentiation of hfs.

All-*trans*-retinoic acid (RA)² is an active retinoid derived from maternal placenta during embryogenesis or from dietary uptake of vitamin A (1). It is commonly used in treatment of

skin diseases such as acne and psoriasis, as well as in chemotherapy for leukemia. A frequent adverse effect from these therapies is RA-induced hair loss (2, 3). However, the mechanistic details of how excess RA arrests hair follicle (hf) growth have not been explored in depth.

Hair follicle induction and growth is dependent on interactions between the epidermis and underlying mesenchyme (4, 5). Several pathways, such as the Wnt, Shh, BMP, and FGF pathways, are essential in these reciprocal signaling events necessary for hair follicle morphogenesis and differentiation (6–10). Initially, a local thickening in the embryonic epidermis forms a hair placode and subsequently, a dermal cell condensate forms underneath the placode. Interactive signaling leads to epidermal downgrowth, with the epithelial cells enveloping the dermal condensate to form the mature dermal papilla. The dermal papilla is responsible for signaling the surrounding epidermal hair matrix cells to differentiate into the hair shaft, inner root sheath, and outer root sheath (9).

Mouse skin develops four hair types (guard, zigzag, awl, and auchene) that can be distinguished by length, the number of medulla columns, and the number of bends in the shaft (11). Guard hairs develop at embryonic day 14.5 (E14.5) during a primary wave of hair growth induced by Eda/Edar signaling (5). A secondary wave at E16.5 gives rise to awl and auchene hairs, and a tertiary wave at E18.5 is responsible for zigzag hair. Noggin and Lef1 signaling are known to be required for induction of secondary and tertiary hair wave. Recently, the molecular basis that establishes the different hair type has begun to be elucidated. Insulin growth factor-1 (Igf1)-mediated signaling, involving Igf1 and several Igf-binding proteins (Igfbps) have been shown to play an important role in the establishment of the hair types (12, 13). Moreover, all dermal papilla of hfs from the first and second wave (guard, awl, and auchene) express the transcription factor Sox2. A characteristic profile of the dermal papilla in zigzag hf (third wave) is the absence of Sox2 expression (14, 15). In addition to the initial hair morphogenesis, throughout life the hair follicle cycles through a growth phase (anagen), regressing phase (catagen), and a resting phase (telogen) (9–11).

^{*} This work was supported by a National Institutes of Health grant from the Intramural Research Program of the NIAMS.

^S This article contains supplemental Figs. S1 and S2.

¹ To whom correspondence should be addressed: Developmental Skin Biology Section, NIAMS, NIH, 50 South Dr., Rm. 1523, Bethesda, MD 20892. Tel.: 301-435-7842; Fax: 301-435-7910; E-mail: morassom@mail.nih.gov.

² The abbreviations used are: RA, retinoic acid; hf, hair follicle; RNA-Seq, RNA sequencing; En, embryonic day *n*; Igf, insulin growth factor; Igfbp, Igf-binding protein; RAR, RA receptor; RXR, retinoic X receptor; AP, alkaline phosphatase; Pn, postnatal day *n*.

This is an Open Access article under the CC BY license.

Excess RA has been shown to induce catagen-like hf regression in human hair cells, and it has been proposed to play a role in the maintenance of hfs and the hair cycle (2, 3). Maintaining a proper balance of RA levels is critical for embryonic development. Retinol is a lipophilic molecule that circulates through the body bound to retinol-binding protein (RBP4). A two-step synthesis converts the molecule to RA. In the first step, cytosolic alcohol dehydrogenases and microsomal retinol dehydrogenases oxidize retinol to retinaldehyde. A second oxidation performed by aldehyde dehydrogenases results in production of RA. Once synthesized, RA can act in either an autocrine or a paracrine manner (1).

Enzymes of the cytochrome P450 26 subfamily (Cyp26a1, Cyp26b1, and Cyp26c1) are involved in the specific inactivation of all-*trans*-retinoic acid to hydroxylated forms such as 4-oxo-RA, 4-OH-RA, and 18-OH-RA. Differential expression of the enzymes responsible for regulating RA catabolism allows for the wide diversity of tissue and temporal specific RA functions. Studies on substrate specificity show that CYP26a1 and b1 are specific for all-*trans*-RA, whereas CYP26c1 metabolizes both all-*trans*-RA and the isomer 9-*cis*-RA (16). Of the three cytochromes, Cyp26b1 is the only enzyme specifically expressed in the dermis surrounding the developing hair follicles (17, 18). Human null and hypomorphic mutations in the gene encoding the RA-degrading enzyme CYP26B1 have been recently reported to lead to skeletal and craniofacial anomalies, including fusions of long bones, calvarial bone hypoplasia, and craniosynostosis (19).

RA acts as a ligand for a heterodimer complex comprised of two classes of nuclear receptors: retinoic acid receptor (RAR) and retinoic X receptor (RXR) (1, 20, 21). In the absence of RA, the RAR-RXR complex recognizes and binds to the DNA retinoic acid response element. The complex recruits co-repressor proteins that inhibit downstream gene transcription. In the presence of RA, the RAR-RXR heterodimer releases the co-repressors and recruits co-activator complexes to the RA response element sequence, initiating transcription of the downstream genes.

To dissect the molecular mechanisms of the impact of RA on hair follicle growth, we deleted *Cyp26b1* in mice. We have characterized the phenotypic effects of excess RA on hair growth and using grafts from *Cyp26b1*^{-/-} showed that normalization of RA levels results in hair follicles resuming growth. Also, to circumvent embryonic lethality, we developed a conditional deletion model by crossing *Cyp26b1f/f* with a dermal-specific Engrailed-1 Cre (*En1Cre*). Analysis of *En1Cre;Cyp26b1f/-* mice has shown that elevated dermal RA levels result in decreased hair follicle density and specific effects on hair type, indicating that RA levels also influence regulators of hair bending. A comparison of transcriptional profiles from the *Cyp26b1*^{-/-} and *En1Cre;Cyp26b1f/-* mice has established new insights into how RA modulates hf type and downgrowth.

MATERIALS AND METHODS

Mice Breeding and Genotyping—*Cyp26b1*^{+/-} and *Cyp26b1f/f* mice were generated and genotyped as previously described (22). The *Cyp26b1f/f* mice were kindly provided by Dr. H. Hamada. No morphological or histological differences were

detected between *Cyp26b1*^{+/-} and WT mice. PCR analysis was used to confirm the deletion of the floxed *Cyp26b1* allele (22). Engrailed-1 Cre (*En1Cre*) mice were purchased from Jackson Laboratories, and the activity of the Cre recombinase was traced by mating with R26R^{LacZ} (Jax3474) (Jackson Laboratories, Bar Harbor, ME). No morphological or histological differences were detected between *En1Cre;Cyp26b1f/+*, *Cyp26b1f/+*, and WT mice. *Cyp26b1f/+* were used as control mice. All of the animal work was approved by the NIAMS Animal Care and Use Committee.

Whole Skin Grafting—A full thickness skin disc (8 mm) excised from E18.5 *Cyp26b1*^{-/-} (*n* = 9) and WT or heterozygote littermate skins (*n* = 9) was applied onto the fascia of the back of immunodeficient nude mice on the right side and on the left side, respectively. Dressings were removed after 7 days. Grafts were excised and divided along the anterioposterior axis after 8, 10, and 21 days. Hairs were plucked from the grafted tissues 21 days after grafting for microscopic analysis. These experiments were performed following National Institutes of Health Animal Care Use regulations with approval under Animal Protocol LCCTP-053.

Northern Blot—mRNA blot for mouse adult tissues were purchased from Clontech and used according to instructions. The probe used was Cyp26b1 mouse coding cDNA. After exposure, hybridized probes were removed by boiling filters in 0.1× SCC, 0.1% SDS. The blot was rehybridized with a cDNA probe for a human β-actin to control for RNA loading and integrity.

Histology, in Situ Hybridization, and Immunohistochemistry—The samples were fixed overnight at 4 °C in 4% paraformaldehyde in 1× PBS, dehydrated, and embedded into paraffin, and 10 μm-thick skin sections were prepared and stained with hematoxylin and eosin. Alkaline phosphatase (AP) staining of whole embryos was performed following the instructions of the Sigma leukocyte alkaline phosphatase kit after fixation with 4% paraformaldehyde for 1 h at 4 °C. AP staining of frozen sections of dorsal skin from E16.5 and E18.5 WT, *En1Cre;Cyp26b1f/-* embryos and grafted skin were performed for a time period of 30 min at 37 °C as instructed by the manufacturer. The slides were rinsed briefly by dipping in H₂O and then counterstained with nuclear fast red solution. The slides were rinsed in H₂O and mounted with mounting medium. Digital photographs were taken at 20×, and the length of the epidermis was measured using ImageJ software. AP activity was detected as a dark blue color in the dermal papilla. Hair density was calculated by dividing the total number of AP-stained hair follicles by the total length of the epidermis. Hair shaft morphology and hair type composition were analyzed under a dissection microscope or at 100× magnification. At least 300 hairs were analyzed for each mouse. To quantify hair density of mice at P7, 3-mm punch biopsies were taken from the dorsal side of three *En1Cre;Cyp26b1f/-* and three control mice. Forceps were used to pluck the hairs from the biopsy punch and spread on microscope slides. A dissecting microscope was used to count the total number of hairs/biopsy punch. A subset of at least 300 hairs from each punch biopsy was analyzed at 20× magnification for hair type composition. An unpaired *t* test (two-tail) was used to assess the significance of the data.

Radioactive *in situ* hybridization on paraffin sections was carried out according to Morasso (23) using [³³P]UTP labeling. The following probes were used: *Cyp26b1* (22) and *Shh*. The *Bmp4* probe was generated to the 2–948 nucleotide residues of the mouse *Bmp4* cDNA (GenBankTM accession number NM007554).

Immunohistochemical analysis was performed on skin sections (10 μ m) that were incubated with primary antibodies overnight at 4 °C. The antibodies and dilutions used were: anti-K5 (1:200; Lifespan Biosciences), anti-pan-keratin (1:10; Abcam), anti-involucrin (1:1000; Covance), anti-Lef1 (1:100; Cell Signaling Technology), anti-Dlx3 (1:250; Morasso Laboratory), anti-Sox2 (1:250; Santa Cruz), and anti-Igfbp5 (1:100; R & D Systems). The secondary antibodies were Alexa Fluor 488 or Alexa Fluor 555 goat anti-mouse, -rabbit, or -guinea pig IgG (1:250; Molecular Probes). The sections were examined using a laser-scanning confocal microscope 510 Meta or Axio Scope A1 (Zeiss).

Microarray and Quantitative RT-PCR Analysis—The dorsal skin samples were homogenized in TRIzol[®] (Invitrogen). Total RNA was extracted using TRIzol[®] reagent (Invitrogen) and a tissue homogenizer with disposable plastic probes (OMNI International, Kennsaw, GA). Microarray analysis was performed on three WT and three cKO animals by the National Institutes of Health NIDDK Genomics Core Facility. RNA quality of the samples was tested using bioanalyzer, and RNA integrity number (RIN) values were above 8.7. 100 ng from each sample was used to amplify the cDNA using NUGEN Applause 3' amplification kit, and biotinylated using Encore Biotin module (NUGEN Technologies) according to the manufacturer's instructions. The samples were hybridized with Affymetrix Mouse 430.2 arrays for 18 h (Affymetrix Inc.) and processed using Affymetrix 450 fluidic stations using Affymetrix hybridization, wash, and staining solutions. The chips were scanned using Affymetrix GeneChip scanner 3000 running Affymetrix (GeneChip Operating Software) GCOS 1.4 version software. Data summarization, normalization, and statistical analysis were performed with Partek Genomics Suite 6.6 (Partek Inc., St. Louis, MO). Differentially expressed genes were selected based on the results of analysis of variance.

To assess the efficiency of cDNA synthesis and labeling, poly(A) RNA was spiked to the samples, and hybridization controls were added according to the manufacturer's instructions. WT samples were averaged and used as a base line to mutant samples. The significantly affected genes ($p < 0.05$ and fold change ≥ 1.5) were selected based on analysis of variance by Partek Pro software (Partek, St. Charles, MO).

Quantitative real time PCR analysis was performed on a MyiQTM single color real time PCR detection system, using iQTM Sybr[®] Green Supermix (Bio-Rad). Individual gene expression was normalized against the RPLPO housekeeping gene. Two-tailed Student's *t* test was used to assess significance of the data.

The primers used were: RAR β forward, AGGACAAGT-CATCGGGCTAC; RAR β reverse, CTGGCATCGGTTC-CTAGTG; *Cyp26b1* forward, CAAGATCCTACTGGGC-GAAC; *Cyp26b1* reverse, GGGCAGGTAGCTCTCAAGTG;

RPLPO forward, ATCAATGGGTACAAGCGCGTC; and RPLPO reverse, CAGATGGATCAGCCAGGAAGG.

RNA Sequencing (RNA-Seq)—RNA-Seq data were generated with an Illumina HiSeq 2000 system. Raw sequencing data were processed with CASAVA 1.8.2 to generate fastq files. Reads of 50 bases were mapped to the mouse transcriptome and genome mm9 using TopHat 1.3.2 (24). Gene expression values Fragments per kilobase of exon per million fragments mapped (FPKM) were calculated using cufflinks/cuffdiff of 1.3.0 (25), which also generates comparison statistics used to determine significantly differentially expressed genes.

Statistical Analysis—All of the quantitative experiments were performed on at least three control and three mutant animals (means \pm S.E.). Statistical analyses were performed on Prism 5 statistical software (GraphPad Software Inc., San Diego, CA), using a *t* test with a significance level of 0.05. * indicates $p < 0.05$; ** indicates $p < 0.01$; and *** indicates $p < 0.001$.

RESULTS

***Cyp26b1* Is Expressed in the Developing Skin and Hair Follicle**—There are three members of the *Cyp26* gene family namely, *Cyp26a1*, *-b1*, and *-c1*. *Cyp26b1* is the only one detected in the developing skin (17, 18, 22). *Cyp26b1* expression was corroborated by Northern blot analysis. A band of ~ 5.5 kb in size was detected in RNA from heart, brain, lung, liver, kidney, and testis tissues (Fig. 1A). We previously showed *Cyp26b1* expression in E17.5 epidermal and dermal fractions (22). Herein, we determined the levels of expression in skin at different developmental stages (E14.5, E16.5, E18.5, and postnatal day 1 (P1)) using real time PCR analysis (Fig. 1B). As previously reported for E17.5 (22), *Cyp26b1* expression levels were higher in the dermal fractions for developmental stages E18.5 and P1. As visualized by *in situ* hybridization, the onset of *Cyp26b1* expression in the developing skin is in the dermis at E14.5, and this expression was maintained after birth. *Cyp26b1* expression commences in the mesenchymal cells surrounding hf buds around E14.5, and its expression becomes clearly associated with dermal condensate cells and dermal papilla cells late in gestation as well as after birth (Fig. 1C).

Loss of *Cyp26b1* Perturbs hf Development—hfs in the mouse pelage begin to develop at E14 (5, 11). We performed whole mount AP staining at E15.5 to determine whether there were any abnormalities in placode induction. No differences were detected in hair placode induction in E15.5 *Cyp26b1*^{−/−} fetuses, which was comparable with that in WT fetuses (Fig. 2A). Furthermore, expression of crucial regulators of hf placode formation analyzed by *in situ* hybridization revealed that *Shh* and *Bmp4* were expressed in WT and *Cyp26b1*^{−/−} skin (supplemental Fig. S1).

Initial characterization through histology showed that most hfs in the mutant *Cyp26b1*^{−/−} embryos arrested at the germ stage. In many instances, hfs were engulfed and found protruding at the skin surface (Fig. 2B, E16.5, right panel). Furthermore, as previously reported, the most down-regulated genes in the microarray analysis of E16.5 *Cyp26b1*^{−/−} mutant skin were genes associated with hf differentiation (Krt12, Krt25, Krt27, Krt28, Krt35, Krt71, Krt73, Krt85, HoxC13, and Lhx2) (22).

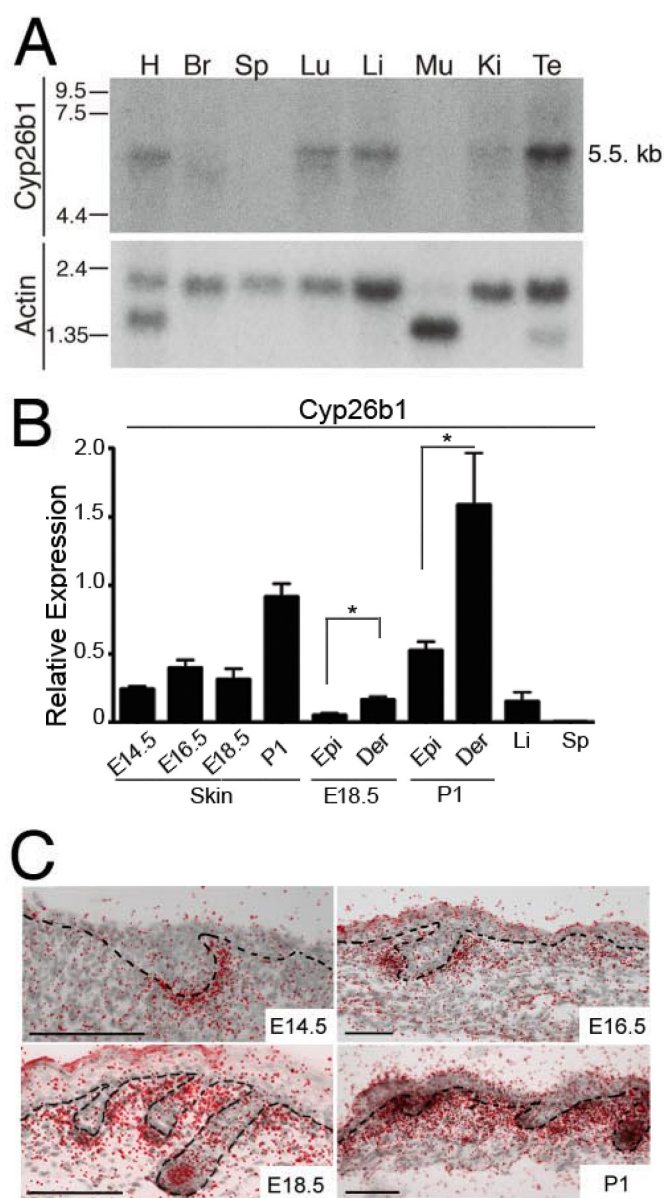


FIGURE 1. *Cyp26b1* expression in tissues. A, Northern blot of 1 μ g of each of mRNA from adult mouse tissues hybridized with a *Cyp26b1* probe. A band of ~5.5 kb in size was detected in RNA from heart (H), brain (Br), lung (Lu), liver (Li), kidney (Ki), and testis (Te) tissues. It was not detected in spleen (Sp) or muscle (Mu). β -Actin signal is present in each lane as a 2-kb band, and two isoforms of β -actin, a 2-kb form and a 1.6-kb form, were observed in heart and skeletal muscle because of hybridization to the α or γ form of actin. B, relative *Cyp26b1* expression in embryonic day E14.5, E16.5, E18.5, and P1 total skin and in epidermal (Epi) and dermal (Der) fractions of E18.5 and P1, determined by real time PCR. Liver (Li) and spleen (Sp) samples from adult mice were used as positive and negative controls, respectively. C, radioactive *in situ* hybridization showed *Cyp26b1* expression in the mesenchymal cells surrounding hf at E14.5 and in the dermis and hfs at E16.5, E18.5, and P1. *, $p < 0.05$.

Ingenuity pathway analysis placed these genes in a network linked to hf development (supplemental Fig. S2), and this is in accordance with the arrested growth of hfs observed in the E18.5 *Cyp26b1*^{-/-} mutant skin (Fig. 2B). Because follicular dermal papilla cells express prominent AP activity during development, we utilized the AP detection to indicate the location of hf in skin. Quantification of the number of hf based on AP detection (Fig. 2, C and D) confirmed that the number of hf was

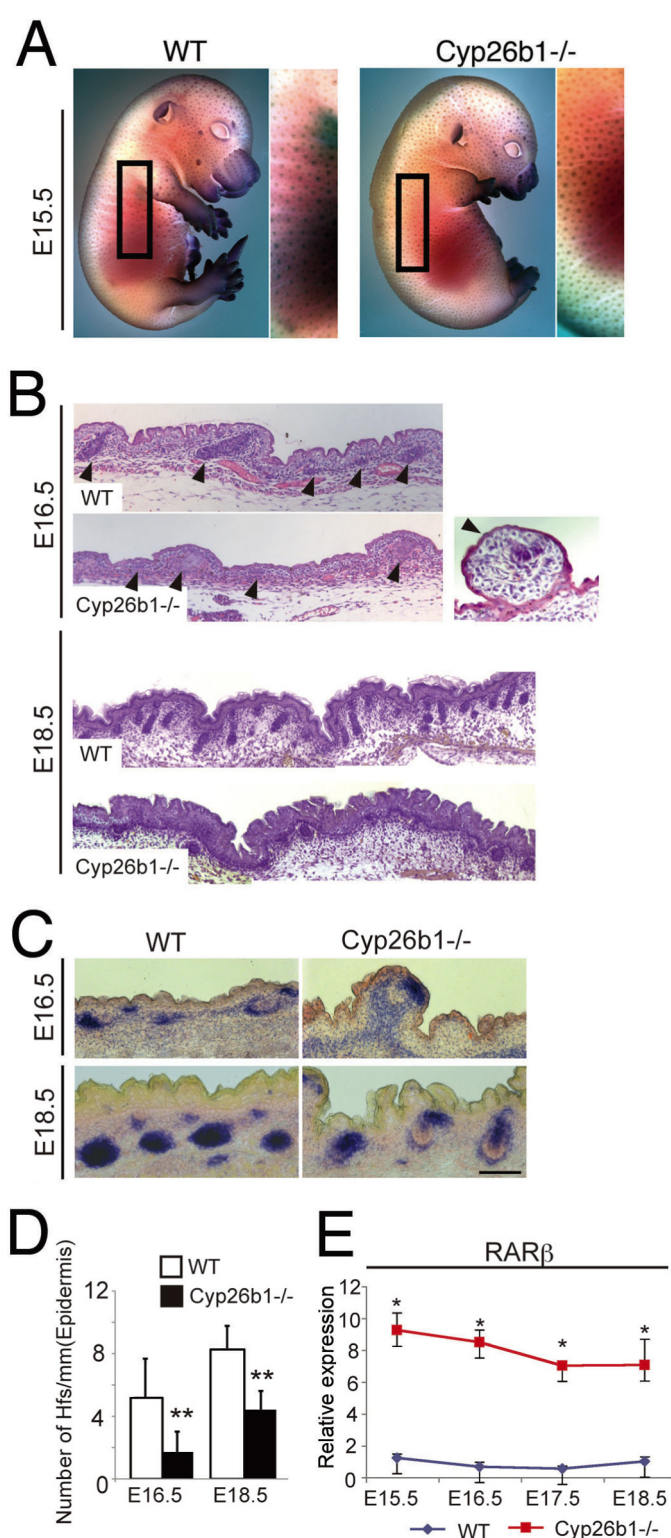


FIGURE 2. Aberrant hf development in *Cyp26b1*^{-/-} fetuses. A, alkaline phosphatase staining pattern at E15.5 was comparable between *Cyp26b1*^{-/-} fetuses and wild-type fetuses. B, histological analysis at E16.5 shows impaired hf development in *Cyp26b1*^{-/-} embryos. High magnification (right panel) shows characteristic engulfed hair follicle detected in mutant skin. By E18.5, hf growth is well developed in WT, whereas hfs arrested at hair germ stage in *Cyp26b1*^{-/-} fetuses. C, AP staining of E16.5 and E18.5 skin sections of WT and *Cyp26b1*^{-/-} skin distinguishes developing hfs. D, quantification of hf number based on AP staining determined diminished hfs number per mm of epidermis in E18.5 *Cyp26b1*^{-/-} skin. E, real time PCR showed that *RARβ* was significantly higher in E15.5 through E18.5 *Cyp26b1*^{-/-} skin compared with WT skin. *, $p < 0.05$; **, $p < 0.01$.

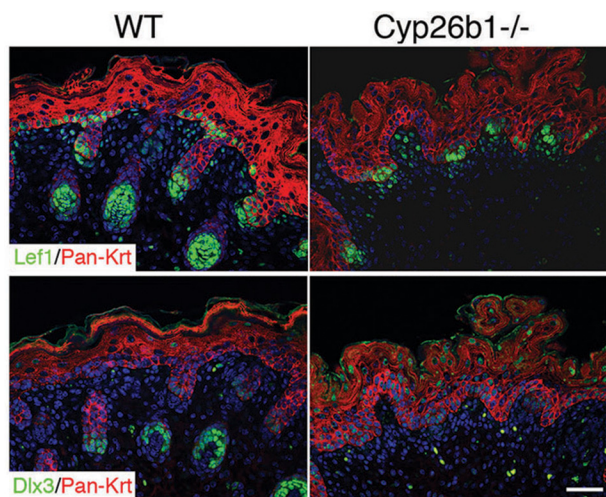


FIGURE 3. Expression of essential regulators of hf development in *Cyp26b1*^{-/-} embryos. Immunofluorescence against Lef1, expression was detected in both E18.5 wild-type and *Cyp26b1*^{-/-} skin. Dlx3 was not detected in the germ-arrested hfs of *Cyp26b1*^{-/-} skin. Pan-keratin (Pan-Krt, red) were used in co-stain. DAPI nuclear staining is shown in blue. Scale bars, 50 μ m.

significantly decreased in *Cyp26b1*-null embryos compared with WT littermates.

Next, we established that the *Cyp26b1*-null skin presented elevated levels of RA when compared with WT skin. RA is a small diffusible molecule, and its concentration is difficult to measure directly in tissues. Because alterations of RA concentration correlate to *RAR β* expression, quantification of *RAR β* has been used to determine levels of RA (22, 26). We examined *RAR β* expression and determined that it was significantly higher in *Cyp26b1*^{-/-} than in WT skin throughout the embryonic period between E15.5 and E18.5 (Fig. 2E).

To establish the cellular and molecular aspects involved in the arrest of hf downgrowth in *Cyp26b1*^{-/-} fetuses, we performed immunofluorescent staining for Lef1, an essential regulator of early hf development, and determined that it was present in growth-arrested hfs in E18.5 *Cyp26b1*^{-/-} fetuses (Fig. 3). On the other hand, Dlx3, a transcriptional regulator of hair differentiation (27), is absent in the mutant hair germs, whereas Dlx3-positive nuclei were detected in the suprabasal layers in *Cyp26b1*^{-/-} skin. Altogether, these data show that although initial placode formation and hf patterning takes place in *Cyp26b1*^{-/-} skin, the number of hfs is significantly reduced and hfs failed to develop beyond the germ stage.

Phenotype of Transplanted *Cyp26b1*^{-/-} Skin Shows Normalization in Skin and hf Differentiation—Because *Cyp26b1*^{-/-} mice die perinatally because of cleft palate malformations, we examined the development of the hfs in *Cyp26b1*^{-/-} skin after birth, by transplanting sections from back skin of E18.5 *Cyp26b1*^{-/-} and littermate control fetuses onto immunodeficient nude mice. By 8 days after grafting, skin differentiation and cornification can be distinguished at the histological level in *Cyp26b1*^{-/-} and control grafted skins (Fig. 4A). In addition, hair development was evident in both *Cyp26b1*^{-/-} and control grafted skin by 10 days after grafting. Three weeks after grafting, fully formed shaft containing hfs are seen in both *Cyp26b1*^{-/-} and control grafted skin. The mutant grafted skin is able to reinitiate and generate hair by 3 weeks.

Immunofluorescence with antibodies to the skin differentiation marker involucrin showed that it was expressed in the suprabasal layers of control and *Cyp26b1*^{-/-} grafted skin, indicating normalized differentiation in the stratified epidermis. The expression appeared to be in broader regions in *Cyp26b1*^{-/-} grafted skin than in control-grafted skin after 8 and 10 days but showed similar pattern to control-grafted skin at 3 weeks. Immunofluorescent staining for Dlx3 showed a correlation with the reinitiation of hair follicle development and Dlx3 expression in *Cyp26b1*^{-/-} graft skin. There are four kinds of hair types in the mouse coat guard, awl, auchene, and zigzag (11). We found all four types of hair in *Cyp26b1*^{-/-} grafted skin as in control skin after 3 weeks (Fig. 4B).

Determination of *RAR β* expression indicated that by 8 days after grafting, the levels of RA have normalized in the grafted mutant skin, even in the absence of the *Cyp26b1* RA-degrading enzyme (Fig. 4C). The development and differentiation of *Cyp26b1*^{-/-} skin and hf after grafting on immunodeficient nude mice indicates that normalization of RA levels is concomitant with reversion of the mutant skin phenotype.

Dermal-specific Excess of RA in Conditional *En1Cre*; *Cyp26b1f*/– Mice Leads to hf Development Defects—Morphogenesis of hair shaft formation and cycling are influenced by signals originating in the dermal papilla (15). Because *Cyp26b1* was robustly expressed in the developing dermal papilla, we utilized *Engrailed1* (*En*)-Cre and mice carrying floxed *Cyp26b1* alleles to delete *Cyp26b1* specifically in dermal papilla and in the dermis of the dorsal skin and systematically investigated the impact of excess RA in hf differentiation after birth. *En1Cre* recombination in dermal condensates and mesenchyme begins by E14.5 (28, 29). Specific *En1Cre* recombination was confirmed using the R26R reporter mice (Fig. 5A). Genotyping revealed *Cyp26b1* deletion by Cre recombinase with a targeted 0.5-kb band in dermis but not in epidermis in *En1Cre*; *Cyp26b1f*/– mice (Fig. 5A, right panel).

Analysis of dermal-specific conditional mouse models such as *Hoxb6Cre*; *Cyp26b1f*/– (22) or with *En1Cre*; *Cyp26b1f*/– (data not shown) determined that there was no significant difference between E18.5 control (*Cyp26b1f*/+) and *cKO* epidermis, as assayed by histology, cell envelope morphology, and barrier function assessed by dye penetration assay. These results support that dermal expression of *Cyp26b1* is not a sufficient effector for the development of the epidermal phenotype observed in *Cyp26b1*^{-/-} skin.

Morphology of developing hfs was comparable between control and *En1Cre*; *Cyp26b1f*/– mice at E16.5; however, hf growth was detected at the peg stage in E18.5 *En1Cre*; *Cyp26b1f*/– mice, compared with that in control (Fig. 5B). Furthermore, as was the case for the E16.5 *Cyp26b1*^{-/-} (Fig. 2B), we observed hfs that were engulfed and found protruding at the skin surface (Fig. 5B, E18.5 panel, arrowheads). We utilized the AP detection to indicate the location of hf in E18.5 *En1Cre*; *Cyp26b1f*/– skin. Quantification of the number of hf based on AP detection (Fig. 5, C and D), confirmed that the number of hf was decreased in E18.5 *En1Cre*; *Cyp26b1f*/– embryos compared with WT littermates. However, the number of hfs in E18.5 *En1Cre*; *Cyp26b1f*/– was higher than those quantified in mutant *Cyp26b1*^{-/-} embryos.

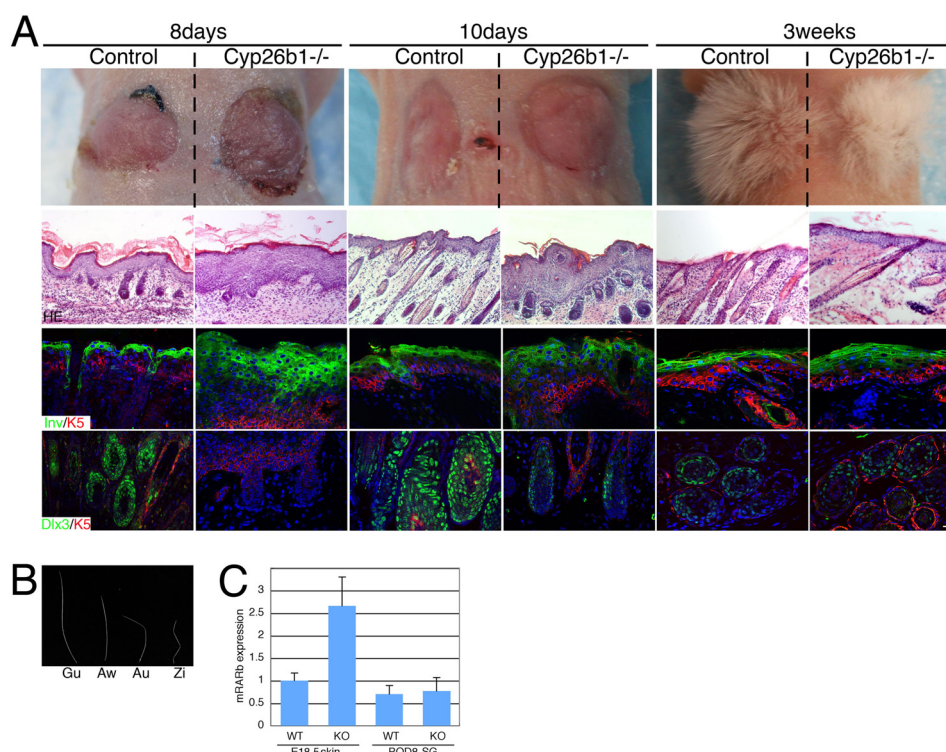


FIGURE 4. Transplantation of E18.5 *Cyp26b1*^{-/-} and littermate skin onto immunodeficient nude mice. *A*, *Cyp26b1*^{-/-} and control grafted skin were similar in gross appearance 8, 10, and 21 days (3 weeks) after grafting. Hematoxylin and eosin (HE) staining showed the formation of cornified layers and the growth of hfs in *Cyp26b1*^{-/-} and control grafted skin. Involucrin (*Inv*) was detected in similar patterns in both grafted skins. Keratin 5 (*K5*) was used in co-stain, and DAPI is visualized in blue. *Dlx3* expression correlated with the reinitiation of hf development. *B*, all four kinds of hair types in mouse coat were observed in *Cyp26b1*^{-/-} grafted skin after 3 weeks. *C*, determination of RARβ expression indicated that by 8 day after grafting, the levels of RA have normalized in the grafted mutant skin. Gu, guard; Aw, awl; Au, auchene; Zi, zigzag; POD8 SG, post operation day 8 skin graft. Scale bar, 50 μm.

We evaluated *RARβ* expression in control, *En1Cre*; *Cyp26b1*^{f/f}, and *Cyp26b1*^{-/-} mice. Real time PCR determined that at E16.5, *RARβ* expression was 3-fold higher in *En1Cre*; *Cyp26b1*^{f/f} than in control skin, whereas it was 8-fold higher in *Cyp26b1*^{-/-} than in control skin (Fig. 5E). By E18.5, skin has differentiated, and it is possible to separate epidermis and dermis fractions. These tissues were utilized to determine *RARβ* expression, which was undetectable in control and *En1Cre*; *Cyp26b1*^{f/f} epidermis but up-regulated by 8.3-fold in *Cyp26b1*^{-/-} epidermis (Fig. 5E). In the dermis, *RARβ* was significantly up-regulated by 2.3-fold in *En1Cre*; *Cyp26b1*^{f/f} mice and 9-fold in *Cyp26b1*-null epidermis compared with control epidermis (Fig. 5E). These results demonstrate that the level of RA in the dermal compartment of the murine embryonic skin directly correlates with hf development and density.

We analyzed the expression of hair transcriptional regulators in *En1Cre*; *Cyp26b1*^{f/f} skin. We utilized *Lef1* as an essential regulator of early hf development and *Dlx3*, a crucial regulator of hf differentiation. The expression of both factors was detected in E18.5 *En1Cre*; *Cyp26b1*^{f/f} mice (Fig. 6). Altogether, these data show that although somewhat delayed when compared with WT, hf development and differentiation takes place in *En1Cre*; *Cyp26b1*^{f/f} skin.

Postnatal Absence of *Cyp26b1* in Dermis and in Dermal Papilla Leads to Impairment of Zigzag hf Development—We investigated whether hf differentiation was affected by deletion of *Cyp26b1* in dermis and in dermal papilla after birth. Histological analysis revealed that hfs appeared to be reduced in

number and that the orientation of random hfs was disturbed (Fig. 7A). We evaluated hf density, which was significantly lower in P7 *En1Cre*; *Cyp26b1*^{f/f} mice than in control (Fig. 7B). This is consistent with a portion of hfs not culminating morphogenesis, as evidenced by the presence of forming hfs engulfed and protruding at the skin surface (Fig. 5B, E18.5 panel). However, we determined that *Sox2* and *Lef1* expression were maintained in P7 *En1Cre*; *Cyp26b1*^{f/f} follicles. The hair coat consists of four different hair types, distinguished by hair length, the number of medulla columns, and the presence and number of bends (11). We analyzed the hf types and found that in *En1Cre*; *Cyp26b1*^{f/f} mice, 33% of hairs presented a single medulla layer but lacked any bending. We termed these zigzag-like (Fig. 7C). The percentages of guard and awl/auchene hfs were similar between control and *En1Cre*; *Cyp26b1*^{f/f}, but zigzag hfs were significantly decreased in conditional mutant mice (Fig. 7C). The length and caliber of each hf type was comparable between control and *En1Cre*; *Cyp26b1*^{f/f} mice (Fig. 7C). These results suggest that the zigzag-like hfs failed to form the bends characteristic of zigzag hfs.

Next, we performed immunohistochemistry to analyze the expression of *Igfbp5*, a marker associated with bending in zigzag hairs, and found that it was comparable between WT and *En1Cre*; *Cyp26b1*^{f/f} hfs (Fig. 7D). We also confirmed that the absence of *Cyp26b1* led to distinct *RARβ* expression in *En1Cre*; *Cyp26b1*^{f/f} skin from P1 to P7 (Fig. 7E), indicating that higher RA levels are present in the cKO skin after birth.

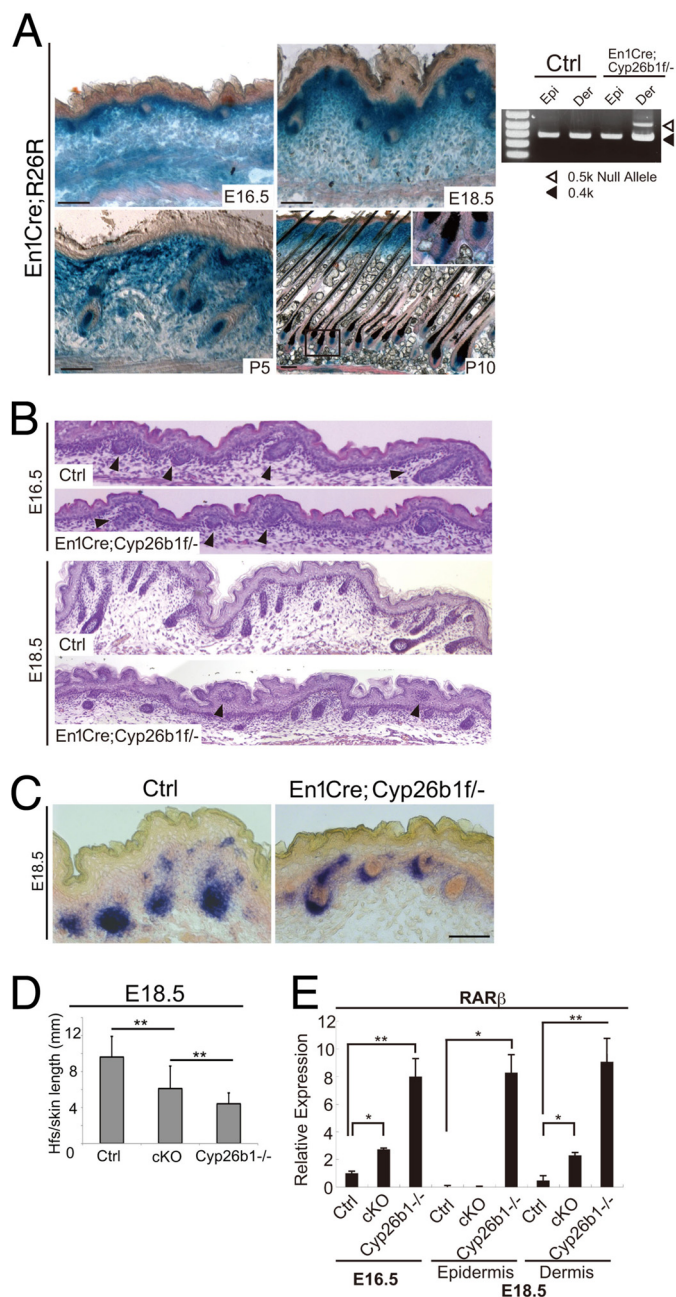


FIGURE 5. Dermal specific deletion of *Cyp26b1* leads to defects in developing hfs. A, LacZ staining of E16.5 to P10 *En1Cre;R26R* skin revealed dermal-specific Cre recombination. Genotyping of E18.5 *En1Cre;Cyp26b1f/-* mice by PCR determined *Cyp26b1* deletion by Cre recombinase in dermis (*Der*) but not in mutant epidermis (*Epi*). B, histological analysis of E16.5 and E18.5 *En1Cre;Cyp26b1f/-* and WT skin shows altered hair follicle development and hf numbers. C, alkaline phosphatase staining pattern in E18.5 *En1Cre;Cyp26b1f/-* and WT skin. D, quantification of hf number based on AP staining determined diminished hfs number per mm of epidermis in E18.5 *En1Cre;Cyp26b1f/-* and *Cyp26b1^{-/-}* skin compared with WT. E, real time PCR determined that *RARβ* expression is significantly up-regulated in *En1Cre;Cyp26b1f/-* and *Cyp26b1^{-/-}* skin at both E16.5 and E18.5. cKO, *En1Cre;Cyp26b1f/-*; Ctrl, control.

Profiling Embryonic *Cyp26b1^{-/-}* Skin and *En1Cre;Cyp26b1^{-/-}* Dermis—We performed RNA-Seq on WT and *Cyp26b1^{-/-}* total skin samples at E16.5. For E18.5 *En1Cre;Cyp26b1f/-* samples, we separated the skin and sequenced the dermal and epidermal fractions. We profiled our three RNA-Seq data sets as well as our previous microarray data from the

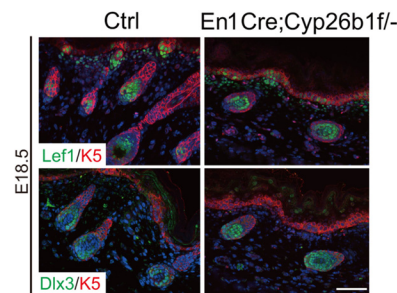


FIGURE 6. Expression of essential regulators of hf development and quantification of hf number and type in *En1Cre;Cyp26b1f/-* skin. Immunofluorescence against Lef1 and Dlx3 expression where detected in both E18.5 WT and *En1Cre;Cyp26b1f/-* skin is shown. Keratin 5 (K5) was used as co-stain. DAPI nuclear staining is shown in blue. Ctrl, control.

complete *Cyp26b1^{-/-}* knock-out at E18.5 (22) (Fig. 8 and Table 1). The complete data sets have been added to the GEO database and have been assigned the number GSE40436. After filtering for genes that were differentially expressed 2-fold or more, all four analyses identified genes known to be involved in hair follicle downgrowth. A high number of keratins were down-regulated in each of the data sets, also consistent with arrest of hair morphogenesis at the hair germ stage (Fig. 8 and supplemental Fig. S2).

In an effort to identify genes and pathways potentially targeted by RA, we used Ingenuity pathway analysis and compared each of the four data sets. Embryonic development, hair and skin development and function and organ development was identified as the top network in all but the E18.5 *En1Cre;Cyp26b1f/-* epidermis samples. The category of hair and skin development and function appeared as one of the highest affected functions in all data sets (supplemental Fig. S2).

Ingenuity pathway analysis showed that a few interconnected canonical pathways were common across the data sets. FGF signaling appeared in the E18.5 complete knock-out as well as the epidermis of the E18.5 dermal conditional knock-out. Wnt signaling was affected in all E18.5 data sets. *RAR* activation was up-regulated in the E18.5 complete knock-out, in E16.5 *Cyp26b1^{-/-}*, and in the dermis from the E18.5 *En1Cre;Cyp26b1f/-* knock-out (Fig. 8, supplemental Fig. S2, and Table 1). The analysis also identified *Runx1*, *Foxe1*, *Sox18*, and *Sox21* as significant down-regulated targets in hair downgrowth and differentiation into distinct hair subtypes in mice.

DISCUSSION

Our previous results demonstrated that persistent high RA concentration in the skin lead to altered embryonic epidermal differentiation and peridermal retention (22). In this study, we used two mouse models to identify the role of endogenously generated RA in hf morphogenesis. The data presented herein support a model in which the control of RA levels in skin is of critical importance for normal hf embryonic downgrowth, differentiation, and hair bending and indicate that the molecular mechanisms involve RA-regulated pathways.

Hf development involves specific patterns of inductive signals between the epithelium and the underlying mesenchyme. Genetic evidence has established significant roles for the Wnt, BMP, and Shh during the interconnected steps necessary for the full morphogenesis and differentiation of the hf (5, 9). Nor-

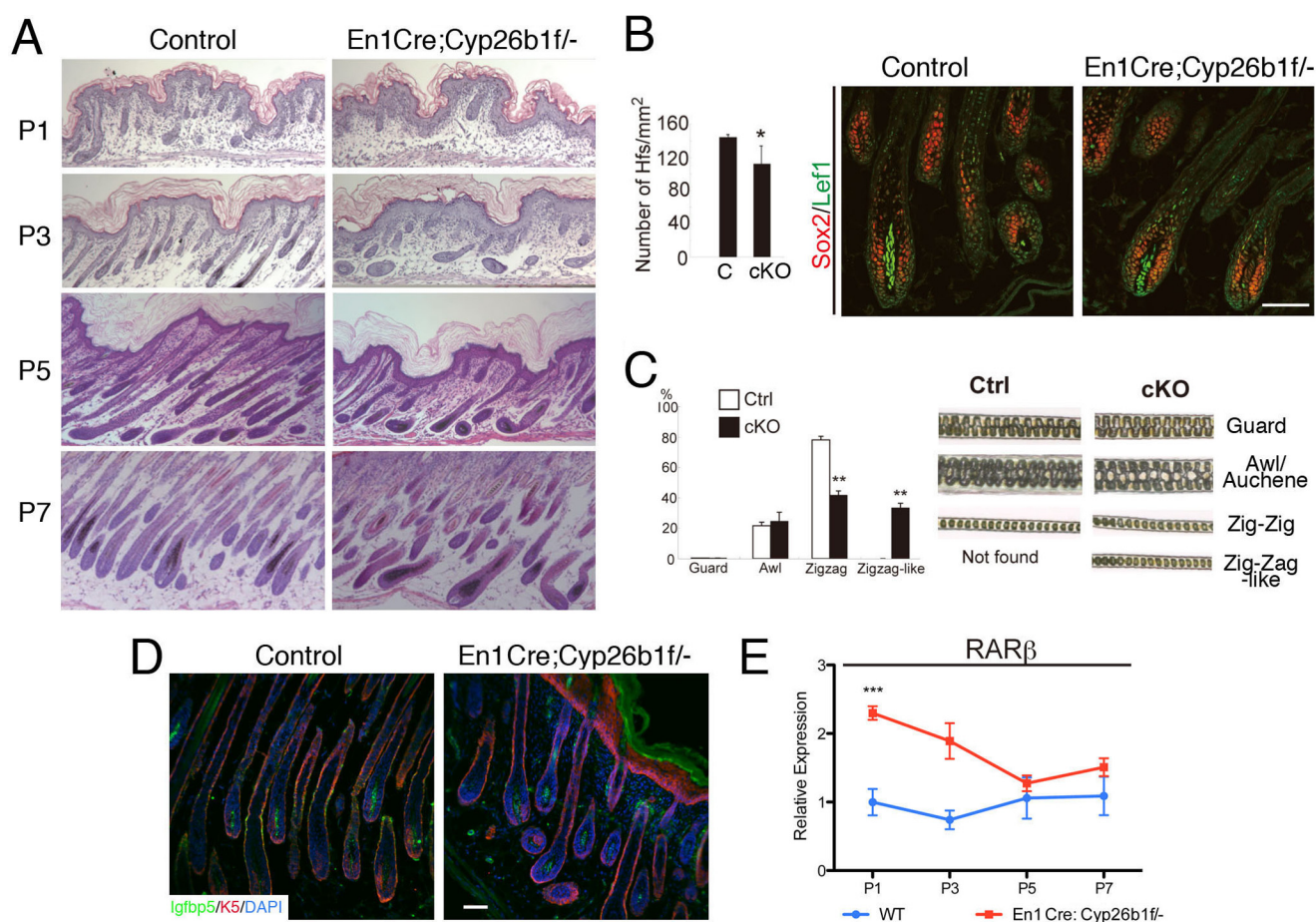


FIGURE 7. hf growth in *En1Cre;Cyp26b1f*^{-/-} mice after birth. *A*, histological analysis of reveals diminished and disoriented hfs in *En1Cre;Cyp26b1f*^{-/-} skin. *B*, hf density is significantly decreased in P7 *En1Cre;Cyp26b1f*^{-/-} skin compared with that in control skin. Sox2 and Lef1 expression is comparable in *En1Cre;Cyp26b1f*^{-/-} skin to WT at P7. *C*, quantitative analysis of hair types at P7 showed that zigzag hairs are significantly decreased in *En1Cre;Cyp26b1f*^{-/-} skin. *Right panel*, analysis of morphology of hair types indicates zigzag-like hairs observed only in *En1Cre;Cyp26b1f*^{-/-} skin. *D*, immunohistochemistry with anti-Igfbp5 shows similar expression pattern in *En1Cre;Cyp26b1f*^{-/-} and WT skin. Keratin 5 (K5) was used as co-stain. DAPI nuclear staining is shown in blue. *E*, real time PCR shows that *RARβ* expression is higher in P1–P7 *En1Cre;Cyp26b1f*^{-/-} skin. Scale bar, 50 μ m. cKO, *En1Cre;Cyp26b1f*^{-/-}. ***, $p < 0.001$. Ctrl, control.

mal development of the epidermal placode and initial formation of the hair germ in *Cyp26b1*^{-/-} and *En1Cre;Cyp26b1f*^{-/-}, in conjunction the detection of expression of *Lef1*, *Bmp4*, and *Shh* in *Cyp26b1*^{-/-} embryos, support that RA signaling is not required for hf placode induction and maturation to the germ stage.

The process of grafting mutant skin on immunodeficient mice was conducive to reinitiation of the hair growth process that had arrested at germ stage in *Cyp26b1*^{-/-} fetuses. The reinitiated hair growth was comparable with that of WT grafted skin. All four-hair types (guard, zigzag, awl, and auchene) developed in the grafted *Cyp26b1*^{-/-} skin. These striking results support that the effect of excess RA is reversible. A significant result that correlates with the reversibility in hf growth capability is the similarity in *RARβ* expression level between *Cyp26b1*^{-/-} and littermate grafted skin at 3 weeks after grafting.

Bioinformatic analysis of the gene expression data sets for *Cyp26b1*^{-/-} and *En1Cre;Cyp26b1f*^{-/-} identifies crucial pathways involved in hair and skin development function as one of the highest affected (Fig. 8, Table 1, and supplemental Fig. S2). Because hf arrest at early germ stage in *Cyp26b1*^{-/-} mice and hf density and bending is affected in *En1Cre;Cyp26b1f*^{-/-} mice, it

was not surprising to find that a highly down-regulated node established by Ingenuity pathway analysis was the group of hair keratin and hf differentiation associated factors (Fig. 8). Previous reports showed the direct control of epidermal keratins by RA (30–32). Because of the complex regulation by RA through multiple RXR/RAR and the variability of the RA response element-binding regions, it remains a challenge to define if this group of clustered hair-specific genes are direct RA-regulated targets during hf development.

Cross-regulation of nuclear hormone receptor and the canonical Wnt signaling pathways have been reported (33). An essential pathway in hf development that we show to be affected in these RA excess mouse models is the Wnt signaling pathway (34, 35). The role of Wnt signaling in placode and dermal condensate formation, hair shaft differentiation, and hair cycling has been established (35). The canonical Wnt pathway utilizes β -catenin as a transducer, where Wnt proteins, after binding the frizzled receptors and the low density related proteins stabilize β -catenin, which is then translocated into the nucleus to act in conjunction with TCF and LEF to activate specific Wnt target genes (36). Several Wnt ligands are expressed in the epithelium and mesenchyme during hf development (37), and Wnt/ β -catenin activity has been demonstrated in both com-

TABLE 1

Summary table of genes involved in hf development, up-regulated, and down-regulated with fold change in each data set

NA, not applicable.

	Cyp26b1 ^{-/-}		En1Cre;Cyp26b1 ^{f/-}	
	E16.5 RNA-Seq	E18.5 microarray	E18.5 RNA-Seq dermis	E18.5 RNA-Seq epidermis
Crabp1	Up-regulated 2.1	Up-regulated 2.7	NA	NA
Crabp2	Up-regulated 2.7	Up-regulated 13.1	Up-regulated 12.4	NA
CTNNA2	NA	NA	Up-regulated 61.9	NA
Ctnnb1	NA	NA	Up-regulated 2533.8	NA
Ctnnd1	Up-regulated 2.3	NA	NA	NA
Ctnnd2	Up-regulated 2.1	Down-regulated - 2.7	Up-regulated 64.9	NA
Dkk1	NA	NA	NA	NA
Dkk4	Up-regulated 2.9	Up-regulated 2.1	NA	NA
Dkk1	NA	Up-regulated 5.4	NA	NA
Dlx3	NA	NA	Down-regulated - 6.2	NA
Eda	NA	NA	NA	NA
Egfr	Up-regulated 2.5	NA	NA	NA
FoxE1	NA	NA	Down-regulated - 30.1	NA
FoxN1	NA	NA	Down-regulated - 8.3	NA
Gata3	NA	NA	Down-regulated - 5.0	NA
Igf-1	Up-regulated 2.3	NA	NA	NA
Igfbp5	NA	NA	NA	NA
Lef1	NA	NA	NA	NA
Lhx2	Down-regulated - 2.2	Down-regulated - 4.1	NA	Down-regulated - 7.9
Lymphotoxin B	NA	NA	NA	NA
Runx1	NA	NA	NA	Down-regulated - 7.1
Runx3	NA	NA	NA	NA
Sostdc1	NA	NA	NA	NA
Sox2	NA	NA	NA	NA
Sox18	NA	Down-regulated - 2.0	NA	Down-regulated - 6.9
Sox21	NA	Down-regulated - 3.7	Down-regulated - 9.7	Down-regulated - 6.8
Stra6	Up-regulated 72.3	Up-regulated 7.7	NA	NA
Wnt4	NA	NA	Down-regulated - 5.3	NA
Wnt5a	NA	NA	NA	Down-regulated - 13.1
Wnt6	NA	Up-regulated 2.1	NA	NA
Wnt7B	NA	Up-regulated 2.1	NA	NA
Wnt10a	Up-regulated 2.1	NA	Down-regulated - 4.1	NA

form primary hair placodes but produce zigzag hairs with no bends (44). Notwithstanding the importance of the *Eda/Edar* pathway in initial regulatory signals of hf development, our results suggest that it is probably independent of RA signaling.

Igfbp5 is one of the first markers associated with bending in zigzag hairs in a regulatory cascade involving *Igf1* signaling (12) and *Krox20* (13). *Igfbp5* expression shifts dynamically from in dermal papilla to in hair matrix, finally moving in the segmental medulla (13, 45, 46). *Igfbp5* is part of a family of proteins, some of which (*i.e.*, *Igfbp3*) have been shown to be regulated by RA in dermal papilla cells (47). Interestingly, no hair phenotype is observed in the triple *Igfbp-3*, *-4*, and *-5* knock-out model (48), and *Igfbp5* expression was unperturbed in *En1Cre;Cyp26b1f/-* hfs, confirming that alternate RA-regulated pathways are involved in the mechanisms that determine bends in hfs.

Wnt signaling also has a role in the patterning of zigzag hairs (49). Overexpression of the Wnt antagonist *Dkk1* in the hair cortex under the control of the *Foxn1* promoter leads to several hf defects featured in Tabby mice, including the absence of zigzag hairs. Moreover, epidermal overexpression of the *Dkk4* Wnt antagonist also leads to a complete loss of zigzag hfs (50). We find up-regulated expression of *Dkk4* in the *Cyp26b1^{-/-}* skin supporting a link between the heightened expression of these secreted Wnt inhibitors and the hair follicle development defects observed in the model with increased dermal RA levels. No significant up-regulation of these inhibitors was found in the *En1Cre;Cyp26b1f/-* dermis to correlate with the specific hair type developmental defect observed in this mouse model. It is noteworthy to mention that although we demonstrate

elevated levels of RA in both *Cyp26b1^{-/-}* and *En1Cre;Cyp26b1f/-* skin, the levels are substantially higher in *Cyp26b1^{-/-}*. Furthermore, three known RA-stimulated genes, *Crabp1*, *Crabp2*, and *Stra6* are only found significantly up-regulated in the *Cyp26b1^{-/-}* model (Table 1). This would support the correlation between progression of hf development and excess levels of RA.

Members of the Runx, Fox, and Sox families of transcription factors are involved in the determination of hair structure. When *Runx1* is specifically inactivated in the epidermis, most zigzag hairs form less pronounced bends that are misoriented and fragile (51). *Foxe1*-null skin develops disoriented and misaligned hair follicles, and *Foxe1^{-/-}* grafted skin presents aberrant the hair shape and septulation (52). Dominant mutations in the *Sox18* transcription factor have been correlated with a reduced number of hairs because of the absence of auchene and zigzag hair types (53, 54). Analysis of our mouse models identified *Runx1*, *Foxe1*, *Sox18*, and *Sox21* as significantly down-regulated targets supporting a role for RA levels in regulation of these factors and a functional role in hair downgrowth and differentiation into distinct hair subtypes in mice.

Cyp26b1 knock-out and dermal-conditional knock-out mouse models were used to systematically identify RA novel target genes and delineate the interactions with signaling pathways in dictating hf differentiation. Our results identify candidates for several key follicular signals, such as *Wnt/β-catenin*, and members of the Runx, Fox, and Sox families of transcription factors, as modulated by RA. Altogether, the data strongly support the conclusion that distinctive levels of RA are neces-

sary to regulate pathways in a fashion that is conducive to hair downgrowth and specification of hair types. Taking into account that 13-*cis*-RA causes hair loss as one of the side effects in humans, and acitretin, one of the retinoids often used for the treatment of psoriasis, results in hair loss as a main side effect, defining the RA-dependent genetic program is the next step to determine the mechanisms involved in RA-induced hair loss.

Acknowledgments—We thank Dr. Olivier Duverger, Julie Erthal, Dr. Jin-Chul Kim, and other members of the Developmental Skin Biology Section for helpful discussions and technical assistance. We also thank Gustavo Gutierrez-Cruz of the NIAMS Genome Analysis Core Facility and the NIAMS Light Imaging Core Facility. For microarray analysis, we thank George Poy and Weiping Chen. We are especially thankful to Dr. Hiroshi Hamada for providing the *Cyp26b1*^{f/f} mice.

REFERENCES

- Rhinn, M., and Dollé, P. (2012) Retinoic acid signalling during development. *Development* **139**, 843–858
- Foitzik, K., Spexard, T., Nakamura, M., Halsner, U., and Paus, R. (2005) Towards dissecting the pathogenesis of retinoid-induced hair loss. All-*trans*-retinoic acid induces premature hair follicle regression (catagen) by upregulation of transforming growth factor- β 2 in the dermal papilla. *J. Invest. Dermatol.* **124**, 1119–1126
- Everts, H. B. (2012) Endogenous retinoids in the hair follicle and sebaceous gland. *Biochim. Biophys. Acta* **1821**, 222–229
- Hardy, M. H. (1992) The secret life of the hair follicle. *Trends Genet.* **8**, 55–61
- Mikkola, M. L. (2007) Genetic basis of skin appendage development. *Semin. Cell Dev. Biol.* **18**, 225–236
- Rendl, M., Lewis, L., and Fuchs, E. (2005) Molecular dissection of mesenchymal-epithelial interactions in the hair follicle. *PLoS Biol.* **3**, e331
- Botchkarev, V. A., and Sharov, A. A. (2004) BMP signaling in the control of skin development and hair follicle growth. *Differentiation* **72**, 512–526
- Enshell-Seijffers, D., Lindon, C., Kashiwagi, M., and Morgan, B. A. (2010) β -Catenin activity in the dermal papilla regulates morphogenesis and regeneration of hair. *Dev. Cell* **18**, 633–642
- Schneider, M. R., Schmidt-Ullrich, R., and Paus, R. (2009) The hair follicle as a dynamic miniorgan. *Curr. Biol.* **19**, R132–R142
- Yang, C. C., and Cotsarelis, G. (2010) Review of hair follicle dermal cells. *J. Dermatol. Sci.* **57**, 2–11
- Duverger, O., and Morasso, M. I. (2009) Epidermal patterning and induction of different hair types during mouse embryonic development. *Birth Defects Res. C Embryo Today* **87**, 263–272
- Weger, N., and Schlake, T. (2005) Igf-I signalling controls the hair growth cycle and the differentiation of hair shafts. *J. Invest. Dermatol.* **125**, 873–882
- Schlake, T. (2007) Determination of hair structure and shape. *Semin. Cell Dev. Biol.* **18**, 267–273
- Driskell, R. R., Giangreco, A., Jensen, K. B., Mulder, K. W., and Watt, F. M. (2009) Sox2-positive dermal papilla cells specify hair follicle type in mammalian epidermis. *Development* **136**, 2815–2823
- Driskell, R. R., Clavel, C., Rendl, M., and Watt, F. M. (2011) Hair follicle dermal papilla cells at a glance. *J. Cell Sci.* **124**, 1179–1182
- Ross, A. C., and Zolfaghari, R. (2011) Cytochrome P450s in the regulation of cellular retinoic acid metabolism. *Annu. Rev. Nutr.* **31**, 65–87
- Abu-Abed, S., MacLean, G., Fraulob, V., Chambon, P., Petkovich, M., and Dollé, P. (2002) Differential expression of the retinoic acid-metabolizing enzymes CYP26A1 and CYP26B1 during murine organogenesis. *Mech. Dev.* **110**, 173–177
- Topletz, A. R., Thatcher, J. E., Zelter, A., Lutz, J. D., Tay, S., Nelson, W. L., and Isoherranen, N. (2012) Comparison of the function and expression of CYP26A1 and CYP26B1, the two retinoic acid hydroxylases. *Biochem. Pharmacol.* **83**, 149–163
- Laue, K., Pogoda, H. M., Daniel, P. B., van Haeringen, A., Alanay, Y., von Ameln, S., Rachwalski, M., Morgan, T., Gray, M. J., Breuning, M. H., Sawyer, G. M., Sutherland-Smith, A. J., Nikkels, P. G., Kubisch, C., Bloch, W., Wollnik, B., Hammerschmidt, M., and Robertson, S. P. (2011) Craniosynostosis and multiple skeletal anomalies in humans and zebrafish result from a defect in the localized degradation of retinoic acid. *Am. J. Hum. Genet.* **89**, 595–606
- Clagett-Dame, M., and Knutson, D. (2011) Vitamin A in reproduction and development. *Nutrients* **3**, 385–428
- Samarut, E., and Rochette-Egly, C. (2012) Nuclear retinoic acid receptors. Conductors of the retinoic acid symphony during development. *Mol. Cell Endocrinol.* **348**, 348–360
- Okano, J., Lichti, U., Mamiya, S., Aronova, M., Zhang, G., Yuspa, S. H., Hamada, H., Sakai, Y., and Morasso, M. I. (2012) Increased retinoic acid levels through ablation of *Cyp26b1* determine the processes of embryonic skin barrier formation and peridermal development. *J. Cell Sci.* **125**, 1827–1836
- Morasso, M. I. (2010) Detection of gene expression in embryonic tissues and stratified epidermis by *in situ* hybridization. *Methods Mol. Biol.* **585**, 253–260
- Trapnell, C., Pachter, L., and Salzberg, S. L. (2009) TopHat. Discovering splice junctions with RNA-Seq. *Bioinformatics* **25**, 1105–1111
- Trapnell, C., Williams, B. A., Pertea, G., Mortazavi, A., Kwan, G., van Baren, M. J., Salzberg, S. L., Wold, B. J., and Pachter, L. (2010) Transcript assembly and quantification by RNA-Seq reveals unannotated transcripts and isoform switching during cell differentiation. *Nat. Biotechnol.* **28**, 511–515
- Johannesson, M., Ståhlberg, A., Ameri, J., Sand, F. W., Norrman, K., and Semb, H. (2009) FGF4 and retinoic acid direct differentiation of hESCs into PDX1-expressing foregut endoderm in a time- and concentration-dependent manner. *PLoS One* **4**, e4794
- Hwang, J., Mehrani, T., Millar, S. E., and Morasso, M. I. (2008) Dlx3 is a crucial regulator of hair follicle differentiation and cycling. *Development* **135**, 3149–3159
- Atit, R., Sgaier, S. K., Mohamed, O. A., Taketo, M. M., Dufort, D., Joyner, A. L., Niswander, L., and Conlon, R. A. (2006) β -Catenin activation is necessary and sufficient to specify the dorsal dermal fate in the mouse. *Dev. Biol.* **296**, 164–176
- Chen, D., Jarrell, A., Guo, C., Lang, R., and Atit, R. (2012) Dermal β -catenin activity in response to epidermal Wnt ligands is required for fibroblast proliferation and hair follicle initiation. *Development* **139**, 1522–1533
- Tomic-Canic, M., Sunjevaric, I., Freedberg, I. M., and Blumenberg, M. (1992) Identification of the retinoic acid and thyroid hormone receptor-responsive element in the human K14 keratin gene. *J. Invest. Dermatol.* **99**, 842–847
- Ohtsuki, M., Tomic-Canic, M., Freedberg, I. M., and Blumenberg, M. (1992) Regulation of epidermal keratin expression by retinoic acid and thyroid hormone. *J. Dermatol.* **19**, 774–780
- Blumenberg, M., Connolly, D. M., and Freedberg, I. M. (1992) Regulation of keratin gene expression. The role of the nuclear receptors for retinoic acid, thyroid hormone, and vitamin D3. *J. Invest. Dermatol.* **98**, 42S–49S
- Beildeck, M. E., Gelmann, E. P., and Byers, S. W. (2010) Cross-regulation of signaling pathways. An example of nuclear hormone receptors and the canonical Wnt pathway. *Exp. Cell Res.* **316**, 1763–1772
- Widelitz, R. B. (2008) Wnt signaling in skin organogenesis. *Organogenesis* **4**, 123–133
- Millar, S. E. (2002) Molecular mechanisms regulating hair follicle development. *J. Invest. Dermatol.* **118**, 216–225
- van Amerongen, R., and Nusse, R. (2009) Towards an integrated view of Wnt signaling in development. *Development* **136**, 3205–3214
- Reddy, S., Andl, T., Bagasra, A., Lu, M. M., Epstein, D. J., Morrissey, E. E., and Millar, S. E. (2001) Characterization of Wnt gene expression in developing and postnatal hair follicles and identification of Wnt5a as a target of Sonic hedgehog in hair follicle morphogenesis. *Mech. Dev.* **107**, 69–82
- DasGupta, R., and Fuchs, E. (1999) Multiple roles for activated LEF/TCF transcription complexes during hair follicle development and differentiation. *Development* **126**, 4557–4568
- Närhi, K., Järvinen, E., Birchmeier, W., Taketo, M. M., Mikkola, M. L., and

- Thesleff, I. (2008) Sustained epithelial β -catenin activity induces precocious hair development but disrupts hair follicle down-growth and hair shaft formation. *Development* **135**, 1019–1028
40. Headon, D. J., Emmal, S. A., Ferguson, B. M., Tucker, A. S., Justice, M. J., Sharpe, P. T., Zonana, J., and Overbeek, P. A. (2001) Gene defect in ectodermal dysplasia implicates a death domain adapter in development. *Nature* **414**, 913–916
 41. Srivastava, A. K., Durmowicz, M. C., Hartung, A. J., Hudson, J., Ouzts, L. V., Donovan, D. M., Cui, C. Y., and Schlessinger, D. (2001) Ectodysplasin-A1 is sufficient to rescue both hair growth and sweat glands in Tabby mice. *Hum. Mol. Genet.* **10**, 2973–2981
 42. Cui, C. Y., Durmowicz, M., Ottolenghi, C., Hashimoto, T., Griggs, B., Srivastava, A. K., and Schlessinger, D. (2003) Inducible mEDA-A1 transgene mediates sebaceous gland hyperplasia and differential formation of two types of mouse hair follicles. *Hum. Mol. Genet.* **12**, 2931–2940
 43. Mustonen, T., Pispä, J., Mikkola, M. L., Pummila, M., Kangas, A. T., Pakkasjärvi, L., Jaatinen, R., and Thesleff, I. (2003) Stimulation of ectodermal organ development by Ectodysplasin-A1. *Dev. Biol.* **259**, 123–136
 44. Cui, C. Y., Hashimoto, T., Grivennikov, S. I., Piao, Y., Nedospasov, S. A., and Schlessinger, D. (2006) Ectodysplasin regulates the lymphotoxin- β pathway for hair differentiation. *Proc. Natl. Acad. Sci. U.S.A.* **103**, 9142–9147
 45. Schlake, T. (2005) Segmental Igfbp5 expression is specifically associated with the bent structure of zigzag hairs. *Mech. Dev.* **122**, 988–997
 46. Schlake, T. (2006) Krox20, a novel candidate for the regulatory hierarchy that controls hair shaft bending. *Mech. Dev.* **123**, 641–648
 47. Hembree, J. R., Harmon, C. S., Nevins, T. D., and Eckert, R. L. (1996) Regulation of human dermal papilla cell production of insulin-like growth factor binding protein-3 by retinoic acid, glucocorticoids, and insulin-like growth factor-1. *J. Cell Physiol.* **167**, 556–561
 48. Ning, Y., Schuller, A. G., Bradshaw, S., Rotwein, P., Ludwig, T., Frystyk, J., and Pintar, J. E. (2006) Diminished growth and enhanced glucose metabolism in triple knockout mice containing mutations of insulin-like growth factor binding protein-3, -4, and -5. *Mol. Endocrinol.* **20**, 2173–2186
 49. Hammerschmidt, B., and Schlake, T. (2007) Localization of Shh expression by Wnt and Eda affects axial polarity and shape of hairs. *Dev. Biol.* **305**, 246–261
 50. Cui, C. Y., Kunisada, M., Piao, Y., Childress, V., Ko, M. S., and Schlessinger, D. (2010) Dkk4 and Eda regulate distinctive developmental mechanisms for subtypes of mouse hair. *PLoS One* **5**, e10009
 51. Raveh, E., Cohen, S., Levanon, D., Negreanu, V., Groner, Y., and Gat, U. (2006) Dynamic expression of Runx1 in skin affects hair structure. *Mech. Dev.* **123**, 842–850
 52. Brancaccio, A., Minichiello, A., Grachtchouk, M., Antonini, D., Sheng, H., Parlato, R., Dathan, N., Dlugosz, A. A., and Missero, C. (2004) Requirement of the forkhead gene Foxe1, a target of sonic hedgehog signaling, in hair follicle morphogenesis. *Hum. Mol. Genet.* **13**, 2595–2606
 53. Pennisi, D., Bowles, J., Nagy, A., Muscat, G., and Koopman, P. (2000) Mice null for sox18 are viable and display a mild coat defect. *Mol. Cell Biol.* **20**, 9331–9336
 54. Pennisi, D., Gardner, J., Chambers, D., Hosking, B., Peters, J., Muscat, G., Abbott, C., and Koopman, P. (2000) Mutations in Sox18 underlie cardiovascular and hair follicle defects in ragged mice. *Nat. Genet.* **24**, 434–437